Analyst

Accepted Manuscript

This article can be cited before page numbers have been issued, to do this please use: B. Paul K, A. K. Panigrahi, V. Singh and S. G. Singh, *Analyst*, 2017, DOI: 10.1039/C7AN00243B.

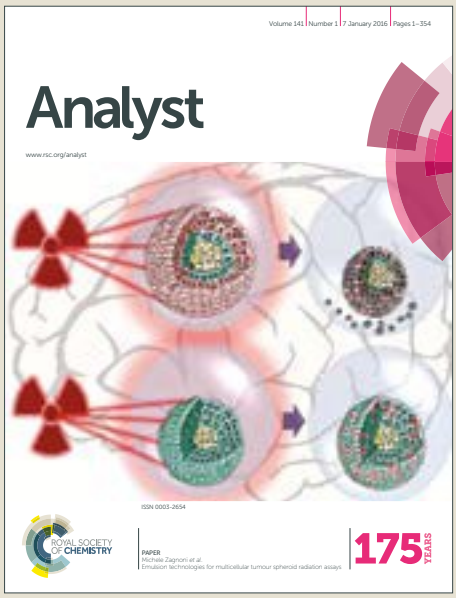

ROYAL SOCIETY OF CHEMISTRY

rsc.li/analyst

View Article Online
DOI: 10.1039/C7AN00243B

Analyst

PAPER

Multi-walled carbon nanotubes - zinc oxide nanofiber based flexible chemiresistive biosensor for malaria biomarker detection

Brince Paul K,‡[a,b] Asisa Kumar Panigrahi,‡[a] Vikrant Singh*[c] and Shiv Govind Singh*[a]

We report fabrication of a flexible, lightweight and disposable multi walled carbon nanotubes (MWCNTs)-zinc oxide (ZnO) nanofiber based chemiresistive biosensor for label free detection of malaria biomarker, histidine rich protein II (HRP2). The sensing platform is formed by depositing nanofibers in between source and the drain electrodes patterned on a thin, flexible polyethylene terephthalate (PET) substrate. The MWCNTs- ZnO nanofibers are synthesized via electrospinning technique followed by calcination process. This approach creates the functional groups on nanofiber surface that are used for the one step immobilization of HRP2 antibodies without further surface modification. The device exhibits good sensitivity of 8.29 kΩ g^{-1} mL, wide detection range of 10 fg mL^{-1} - 10 ng mL^{-1}, and specific towards the targeted HRP2 biomarker. To the best of our knowledge, this is the first report on flexible chemiresistive biosensor explored for the detection of malaria biomarker and can be extended in the future to several other biomarker detection systems towards smart point-of-care (POC) diagnostics.

Received 00th January 20xx,
Accepted 00th January 20xx

DOI: 10.1039/x0xx00000x

www.rsc.org/

Introduction

Malaria is one of the leading life threatening infectious disease in underdeveloped and developing countries. Each year, about 300 to 500 million people are at a high risk of malaria infection.[1] Malaria is caused by different type of Plasmodium protozoans species.[2] Among these, Plasmodium falciparum (P. falciparum) is the most severe form of malaria and interest is focused on the detection of Plasmodium-specific proteins.[3,4] One of these, falciparum histidine-rich protein2 (PfHRP2) based assays shows the better sensitivity and specificity compared to those of other proteins for the detection of P. falciparum. There are several modern methods to diagnosis malaria including microscopic technique,[5-7] molecular diagnostic methods,[8,9] microarrays,[10] flow cytometry,[11,12] automated blood cell analyzers,[13] mass spectrophotometry,[14] lamp technique[10] and Polymerase Chain Reaction (PCR) based detection.[9] These methods are time consuming, expensive and require a trained technician. In order to overcome this, researchers have explored malaria detection based on nanotubes,[1] nanofibers,[15] magneto[16] and optofluidic methods.[17] However, the need for simple, sensitive, flexible and portable biosensing platforms is of great interest in point of care (POC) diagnosis.

One diamensional (1D) metal oxide semiconducting materials have recently garnered much attention in point of care diagnostics (POC) due to their high thermal, mechanical and chemical stability in nanoregime.[18,19] Besides this, 1D semiconducting materials provide faster electron transport as compared to the bulk.[20] Among them, Zinc Oxide (ZnO) are particularly stimulating because of their high surface to volume ratio, non-toxicity, biocompatibility, high electron transfer capability and free-exciton binding energy (60 me V).[21,22] Moreover, the high isoelectric point (IEP=9.5) of ZnO provides an additional benefit for direct immobilization of the biomolecules having low isoelectric point.[23] Numerous 1D Zinc Oxide materials based biosensors have been reported for the detection of cancer biomarkers, DNA, uric acid and glucose.[24-31] However, high resistivity and requirement of additional surface modification for protein conjugation limit their applications towards the development of flexible and highly sensitive point of care device.[32] In this context, doping or incorporation of ZnO nanostructures with suitable material is considered very important for enhancing the sensing properties.[33,29] Carbon nanomaterial's such as carbon nanotubes (CNTs), graphene and reduced graphene oxide (RGO) nowadays have gained much attention in the field of biology, due to their unique physical and chemical properties. However, aggregation of sheets in aqueous solution due to hydrophobic nature of RGO, difficulty in isolating single layer of graphene and its tendency to curl, fold, and corrugate are the major drawbacks.[34] Biosensors based on well aligned, uniformly distributed CNTs have been reported.[35] CNTs, as a grafting material in to metal oxide, has been applied in developing highly sensitive biosensors.[36,37] Furthermore, CNTs doped ZnO and ZnO-MWCNTs nanostructures shows enhanced sensing characteristics than that of multiwalled carbon nanotubes (MWCNTs) or ZnO alone.[38,39] There have been few reports in literature on ZnO-MWCNTs based electrochemical sensors.[40-45] However, the electrical detection technique is preferred over other detection methods due to their potential for miniaturization, simple and convenient

[a] Department of Electrical Engineering, Indian Institute of Technology, Hyderabad, Telangana-502285, India. Email: sgsingh@iith.ac.in; Tel:+91-040-23016079.
[b] Department of Biomedical Engineering, Indian Institute of Technology, Hyderabad, Telangana-502285, India.
[c] School of Medicine, University of California Davis, USA. Email: vssingh@ucdavic.edu
‡ These authors contributed equally.
†Electronic Supplementary Information (ESI) available: [details of any supplementary information available should be included here]. See DOI: 10.1039/x0xx00000x

View Article Online
DOI: 10.1039/C7AN00243B

measurements.[35,46] In a previous study by our group, Durga Prakash et al.[47,48] developed SU8 photoresist-based biosensor for the detection of cardiac biomarker. The concept is based on the loading of MWCNTs in to SU8 photoresist to enhance the conductivity of SU-8 nanofiber and the transduction mechanism relies on change in conductivity due to surface stress caused upon the binding of the biomarker. However, it was necessary to treat the nanofiber with acids in order to increase the surface reactivity. In the current study, MWCNTs doped metal oxide semiconducting nanofibers were synthesized for the development of chemiresistive biosensor. The sensing mechanism depends on the change in electrical resistance due to modification of semiconducting properties of the metal oxide nanofiber upon the analyte interaction. The key here is that the calcination process during the synthesizing of nanofibers generate abundant functional groups that are effective for the immobilization of antibodies without further surface treatment.

Nowadays, flexible material based platform technologies have attracted significant interest in POC diagnostics because of their light weight, portability, flexibility, inexpensive and readily availability of material around the world.[49] There have been many efforts to fabricate POC devices on flexible substrates based on colorimetric, fluorometric, and electrochemical approaches.[50-54] However, one-dimensional nanostructure based chemiresistive transducer have great potential in POC diagnosis because of their simple measurement, miniaturization and superior biosensing performance.[46] Therefore, the present study reports a label-free flexible chemiresistive immunosensor to detect malaria antigen PfHRP2 using 1-D MWCNTs-ZnO nanofibers synthesized by electrospinning method. Among the various methods, electrospinning is considered to be one of the most versatile and cost effective approach for synthesis of one dimensional nanofibers.[55] To the best of our knowledge, this is the first report on flexible chemiresistive based immunosensor explored for direct detection of PfHRP2 malaria antigen.

Experimental

Materials and apparatus

Zinc acetate dehydrate ($Zn(CH3COO)_2 2H_2O$,99%), Polyacrylonitrile (PAN, MW=150,000), N,N dimethylformamide(DMF), Phosphate Buffer Saline (PBS, pH 7.4) tablets, N-ethyl-N-(3-dimethylaminopropyl carbodiimide) (EDC), N-hydroxysuccinimide (NHS) and Bovine serum albumin (BSA) were purchased from Sigma- Aldrich, USA. Pristine MWCNTs (diameter: 20–70 nm and length: 1-10µm) was obtained from Reinste Nano Ventures. Immunoglobulin G (IgG) and creatinine antigen were procured from Abcam, India.

The synthesized MWCNT-ZnO nanofibers were characterized using field emission scanning electron microscopy (FE-SEM; Ultra 55,Zeiss, Germany) , high resolution-transmission electron microscope(HR-TEM, FEI-Tecnai G2- F30, 300 KV) ,Energy Dispersive X-ray spectroscopy(EDX; Oxford Instruments), X-ray diffraction measurements (XRD; XPert Pro, PAN Analytical, Netherlands, X-ray system with Cu Kα radiation and λ = 1.54 A˚), X-ray photoelectron spectroscopy (XPS), UV-visible spectroscopy (UV-Vis; Perkin Elmer- Lambda 750) and fourier transform infrared spectroscopy (FT-IR; Bruker-Germany, Model-Vertex 80). All electrical measurements were carried out using Keithley 4200-SCS source measurement units and Cascade Microtech Summit 11000M Probe station.

Electrode array patterning and nanofiber synthesis

In this study, polyethylene terephthalate (PET) of 300 µm thickness was used as a flexible substrate for the fabrication of the flexible chemiresistive biosensing platform. Prior to pattering of electrode array, the PET substrate ultrasonically cleaned with acetone, isopropanol (IPA) and DI water respectively. Au layer of thickness 100 nm was deposited on the Cr (10nm) adhesion layer by

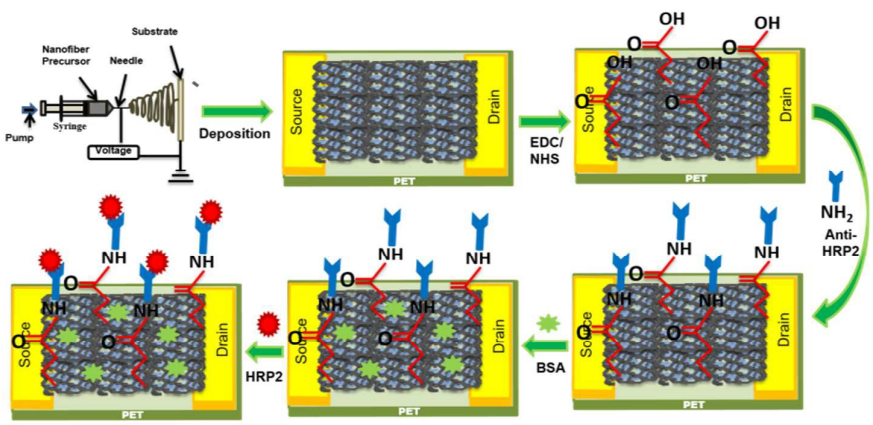

FIG. 1 Schematic representation of the stepwise fabrication process of flexible chemiresistive biosensor for HRP2 malaria biomarker detection.

View Article Online
DOI: 10.1039/C7AN00243B

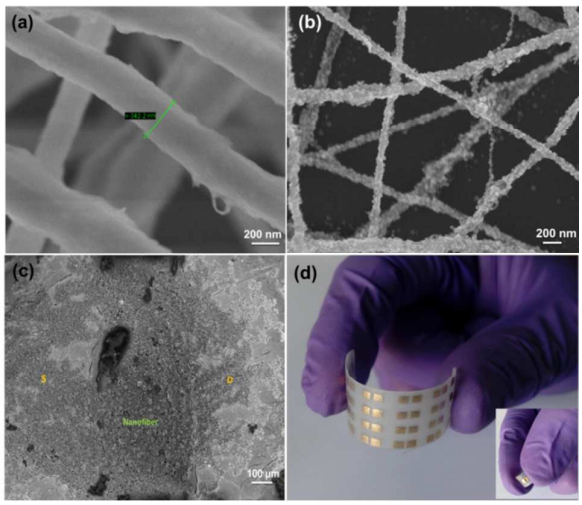

FIG. 2 FESEM image of (a) synthesized nanofiber before calcination (b) nanofiber after calcination (d) device after nanofiber deposition. (c) Optical image of array of fabricated device on PET. Inset shows single device after nanofiber deposition.

DC sputtering. The pattering of the source and drain gold electrodes of width 2 mm and 250 µm of channel gap was performed by a conventional photolithography and liftoff process. MWCNTs- ZnO nanofibers were synthesized using the electrospinning method. In brief, a known quantity of MWCNTs was ultrasonically dispersed in N, N-dimethylformamide (DMF) for 15 minutes. After this, 8 wt% of polyacrylonitrile (PAN, MW=1, 50,000) was added and the mixture was vigorously stirred for 2 hours at 65˚C. To this solution, 4 wt% of zinc acetate dehydrate was added and left aside for stirring for 3 hour at about 60ºC. The weight percentages of MWCNTs were optimized to 4 wt% to obtain a uniform nanofiber without hindrance of electrostatic repulsion.weight percentages of zinc acetate dehydrate and PAN were also optimized to obtain a bead free fiber. The prepared homogeneous precursor solution was then loaded into 5 ml syringe with 26 gauge metallic needle for electrospinning. Electrospinning parameters such as flow rate (40 µL/min), electric field (2 kV/cm) were optimized to get a nanofiber mat. The obtained nanofiber mats were calcined in air at optimized critical temperature (400 ^{o}C) for 2 h (heating rate: 5 °C min^{-1}) to get uniform CNT-ZnO nanofiber without decomposition of MWCNTs. Calcination of nanofiber at higher temperature enabled the defective carbons to be functionalized in to carboxylic groups, which can be utilized for covalent conjugation of molecules.[56,57] Zinc oxide nanofibers without using MWCNTs were also prepared for comparison.

Device fabrication and surface functionalization

The proposed flexible device was fabricated by drop casting 10 µL of MWCNTs-ZnO nanofiber suspension across a pair of 250 µm apart microfabricated gold electrodes. nanofiber suspension was prepared by sonicating MWCNTs-ZnO nanofiber mat in DMF (0.5 mg mL^{-1}) for 1 h. The drop-casted devices were then annealed at 65 °C for 1h to remove the trapped water molecules. For antibody (Anti-HRP2) functionalization, the drop casted MWCNTs-ZnO nanofibers were treated with linker solution containing 0.4 M EDC (coupling agent) and 0.1 M NHS (activator) for 4h to activate the carboxylic(–COOH) groups on the nanofiber surface. After washing with PBS, the MWCNTs-ZnO nanofiber channels were incubated overnight with 10 µL of anti-HRP2 antibody (200 µg/mL) at 4°C to obtain the desired Anti-HRP2/MWCNTs-ZnO device. The antibodies were covalently immobilized on the nanofiber surface via strong amide bonds formed between the amine groups of the antibodies and activated carboxylic groups of the MWCNTs-ZnO nanofiber. The device was then thoroughly washed with PBS (pH 7.0) to remove any unbound antibodies and dried. It was further incubated with 1wt% of bovine serum albumin (BSA) for 1h at 37 ^{o}C to block the nonspecific binding sites followed by washing with PBS (pH 7.0). To investigate the sensing performance of the device, it was incubated with a 10 µL of varying concentrations of target HRP2 antigen for an optimized period of 30 min followed by washing with PBS (pH 7.0), air-drying, and resistance measurement. The stepwise fabrication process of the device is schematically represented in Fig. 1.

Results and discussion

The FESEM image of synthesized PAN/Zn (CH3COO) $_2$ /MWCNTs composite nanofibers before calcination is shown in Fig 2a. The electrospinning parameters and weight percentages of PAN polymer, zinc acetate were optimized to get uniform, bead free continuous fibers with diameters in the range of 300–400 nm. The weight percentage of MWCNTs was also optimized to 4 wt % to

View Article Online
DOI: 10.1039/C7AN00243B

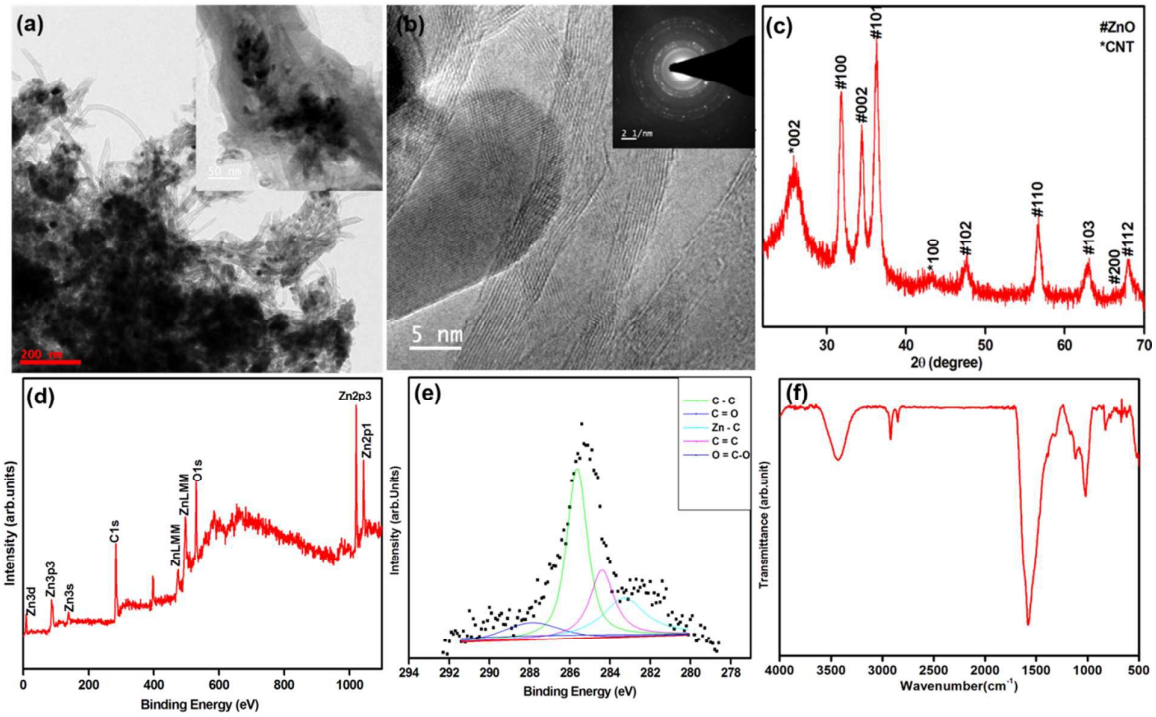

FIG. 3 (a) TEM image of nanofiber mat; Inset showing single nanofiber (b) HRTEM showing interface of the nanofiber; Inset shows SEAD pattern (c) XRD results of synthesized nanofiber conducted between 2θ angles 20° and 70° (d) XPS survey spectra of synthesized nanofiber (e) C1s core level spectra of the nanofiber (f) FTIR spectra of synthesized nanofiber.

.

avoid electrostatic repulsion and segregation at the grain boundaries. After calcination, MWCNTs- ZnO nanofibers are formed due to the oxidative decomposition of $Zn(CHCOO)_2$ and degradation of PAN. The critical calcination temperature was optimized to 400 °C to avoid any decomposition of carbon nanotubes. The diameter of the resultant ZnO-MWCNTs nanofibers shrunk to about 180-200 nm (Fig. 2b). Fig. S1† shows the EDX spectra and mapping of nanofibers before and after the calcination.The significant decrease in wt % of carbon in calcined nanofibers can be attributed to the degradation of PAN polymer. The FESEM image of fabricated device (Fig. 2c) reveals the deposition and orientation of the drop casted nanofiber mat across the source and drain Au electrodes. Fig. 2d shows an Optical image on array of fabricated devices on a PET substrate to demonstrate the mechanical flexibility of the device. A single device fabricated on flexible PET substrate is shown in inset Fig. 2d. Fig. 3a shows the TEM image of MWCNTs-ZnO nanofiber mat and and the inset figure shows the TEM image of single MWCNTs-ZnO nanofiber. Fig. 3b is the corresponding HRTEM, which further proves the formation of the interface between CNT and ZnO in MWCNTs-ZnO nanofiber after calcination. The selected area electron diffraction (SAED) pattern of the MWCNTs-ZnO nanofiber (inset of Fig. 3b) featuring its polycrystalline nature.

The results of XRD studies of synthesized nanofibers conducted between 2θ angles 20° and 70° are shown in Fig. 3c. The characteristic diffraction peaks of ZnO phase at 2θ =31.7 º, 34.4 º, 36.28 º, 47.5 º, 56.6 º, 62.8 º, 67.9 º and 69.1 º are indexed as (100), (002), (101), (102), (110), (103), (200), and (112) planes respectively, while the typical diffraction peaks at 2θ =26 º and 43º is indexed as (002) and (100) graphitic plane of MWCNTs.[55] To further reveal the surface composition and element chemical state, XPS spectra of the synthesized nanofiber were spectra were studied. The survey XPS spectra of Synthesized MWCNTs-ZnO nanofiber sample are shown in Fig. 3d, which confirms the presence of Zn, O, and C elements. Fig. 3e reveals the core level XPS spectra of C 1s region for synthesized nanofiber. The peaks located at around 284.4, 286.3 ,287.9 and 288.8 ,290.6can be ascribed to C=C, C–C, C-O-C, C=O and O=C-O (carboxyl) functional groups, respectively.[58]

To confirm the available functional groups on MWCNTs-ZnO nanofiber surface for the immobilization of proteins, FTIR studies were performed (Fig. 3f).The peak seen at 522 cm^{-1} is due to Zn-O bending while the peak at 3434 cm^{-1} corresponding to Zn-OH stretching in the MWCNTs-ZnO nanofiber. The peak observed at 1100 cm^{-1} is due to the presence of O-C group. The peak present near at 1500 cm^{-1} is corresponding to C=C bending whereas, the peak at 1384 cm^{-1} is due to C-O-H bending in the sample. The peak found at 3752 cm^{-1} and 3434 cm^{-1} are assigned to hydroxyl and OH stretch from carboxyl groups present in the sample.[59] The peak

View Article Online
DOI: 10.1039/C7AN00243B

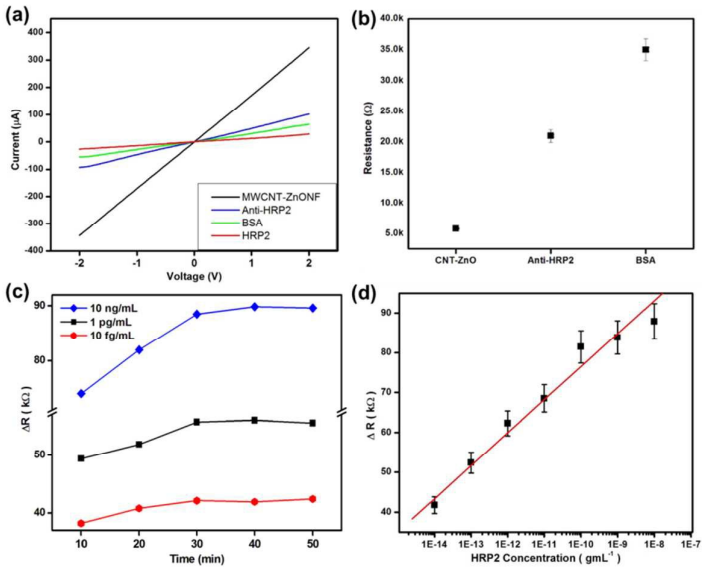

FIG. 4 (a) Current-Voltage (I-V) characteristics curves of the device at different stages of fabrication (b) corresponding resistance curve. (c) Optimization of HRP2 incubation time. (d) Calibration plot of HRP2 detection on fabricated chemiresistive biosensor.

observed around 2900 cm^{-1} is attributed to the H–C stretch mode of H–C=O in the carboxyl group.[59,60] All the peaks are slightly shifted due to the effect of doping. The band gap energy of nanofibers were obtained from (αhυ)2 vs Photon energy(hυ) plot (Fig. S2†). The direct bandgap energy (E_g) can be estimated from the expression $(\alpha h\upsilon)^2=C(h\upsilon- Eg)$. Where, α is the absorption coefficient and C is a constant. The less band gap value obtained for CNTs doped ZnO nanofibers (E_g =2.92) as compared to that of pure ZnO nanofibers (E_g=3.14) indicates the formation of Zn-O-C bonds.[61]

The device characterization at each step of fabrication and subsequent surface modification during fabrication were carried out by monitoring current–voltage (I-V) characteristics in the range from – 2.0 V to + 2.0 V. The corresponding resistance was calculated by taking the inverse of the slope of I-V characteristics. Fig. S3a† shows the I-V curve and Fig. S3b† shows the corresponding resistance curve obtained for the devices fabricated with CNTs doped and un doped ZnO nanofibers in the voltage range of -2.0 V to +2.0 V. An increase in source – drain current (I_{sd}) was observed for the CNTs doped ZnO nanofiber device as compared to the ZnO nanofiber device. The enhancement in electrical properties of the carbon nanotube–zinc oxide composite nanofibers were achieved through two factors: The first of these is related to the reduced Schottky barrier due to the suppression of grain-boundary scattering as a result of the existence of MWCNTs at the grain boundary, and the other is due to the incorporation of carbon into the ZnO lattice (through direct and indirect chemical bonding such as C–Zn–C, Zn–C, O–Zn–C, Zn–O–C and C–Zn–Zn), which can behave as a donor in ZnO crystal lattice.[61,62-65] Fig. S4† shows the resistance (R) behavior of the five different CNTs-ZnO nanofiber device fabricated with similar conditions. The relative standard deviation (RSD) was found to be 8.44 %, which suggest the good stability and reproducibility of the fabricated devices.

Fig. 4a shows the I-V characteristics of the fabricated device after successive treatment with HRP2 antibody, BSA and antigen, respectively. A decrease in current was observed upon covalent attachment of HRP2 antibodies on the device, which further decreased on treatment of BSA blocking agent. As shown in Fig. 4b, the resistance of the device increased with each step of device functionalization. Two possible mechanisms can be postulated as the origin of the change in conductance of nanofiber upon bio-molecular functionalization: one is due to the adsorption of ionized atoms present on the biomolecule's surface, which may modify the depletion region of nanofiber depending on the net charge polarity, and the other is due to the alteration of the electrostatic gate potential as a result of the adsorbed charged molecules .[64,65-67] The device was incubated with 10 µL of each concentration of HRP2 for an optimized incubation time, at room temperature, washed thoroughly with PBS (pH 7.0), dried followed by measuring I-V characteristics. To optimize the incubation period for HRP2, the change in resistance ΔR of the device was measured with the incubation time for three different HRP2 concentrations (Fig. 4c). (ΔR=R-R0, where R0 and R is the resistance of the device measured before and after exposure to HRP2 antigen, respectively) The change in resistance ΔR increased with incubation time and saturated after an incubation period of 30 min. Therefore, 30 min incubation period was used in all subsequent experiments. The increasing trend of the resistance can be attributed to the formation of immuno-complexes between HRP2 and anti-HRP2 antibodies that scatters the charge carriers at the nanofiber interface due to the electrostatic gating effect.[68] Fig. 4d shows the

View Article Online
DOI: 10.1039/C7AN00243B

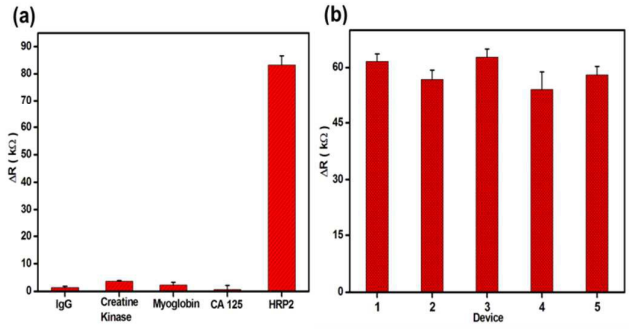

FIG. 5 (a) Response of the chemiresistive biosensor towards nonspecific analytes with respect to HRP2 antigen. (b) The reproducibility of the four different devices towards 1pg mL^{-1} of HRP2 with similar conditions.

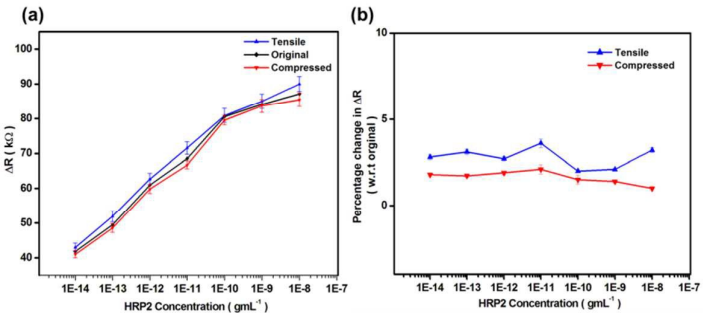

FIG. 6 (a) Response of the device in terms of change in resistance ΔR at different HRP2 concentrations, under tension (blue), compression (red) and unbend state.(b) Percentage change in resistance ΔR with respect to original unbend of the device at different HRP2 concentrations.

response curve obtained between the change resistance ΔR and log concentration of HRP2 in the range of 10 fg/mL to 10 ng/mL. The device exhibited a linear response in ΔR over the range of HRP2 concentrations varying from 10 $fgmL^{-1}$ to 10 $ngmL^{-1}$ with a sensitivity of 8.29 kΩ g^{-1} mL (R^2=0.978). The detection limit of the device was calculated to 0.97 fg mL^{-1} using the formula 3σ/m, where m is the slope of the linear curve and σ is standard deviation of the blank measurement.

To investigate the specificity of the CNTs-ZnO nanofiber device, the device responses towards non-specific antigen such as immunoglobulin G (IgG), Creatine kinase, Myoglobin and CA125 was monitored. Fig. 5a shows the change in resistance ΔR of the device on exposure to 10 ng/mL of IgG, Creatine kinase, Myoglobin and CA125 with respect to HRP2. The variation of change in resistance ΔR due to the interfering substances was less than 4.5% with respect to HRP2 antigen. This is due to the non-occurrence of immunoreaction on the device.[67] However, the response in change in resistance ΔR for nonspecific molecule was significantly smaller in comparison to a response in change in resistance ΔR for HRP2 protein. These results clearly imply that the device is highly specific for HRP2 and does not cross react with other interferants. The reproducibility was investigated by monitoring response ΔR towards 1 pg mL^{-1} of HRP2 using five different devices under similar conditions (Fig. 5b). The relative standard deviation (RSD) was found to be as 6.14 %, which suggest good reproducibility and precision of the devices. The repeatability of the device was performed using repeated measurements for 10 fg/mL of HRP2 at same conditions. Even after 10 times of repeated measurements, the device showed stable response with a low relative standard deviation of 1.15 % (Fig. S5†). The stability of the same device was checked for 15 days at a regular interval of 3 days (Fig. S6†). The decrease in the value of change in resistance ΔR was found to be about 5.8 % after 15 days. The decrease in the response may be due to the denaturation of biomolecules.

It is essential to study the effect of strain on sensor performance to eliminate or incorporate the strain effect on the bimolecular detection and sensor integration for the development of robust, reliable and ultrasensitive flexible sensors. For this flexibility studies, one end of the device were affixed on a fixed sample holder with another end to a movable arm. Sample holder with movable arm was used to stretch or compress the device by changing the bending direction of substrate. It was observed that the resistance of the device increases with tensile strain and decreases with compressive strain with respect to original unbend state. The magnitude of strain can be calculated according to Xinqin Liao et al.'s work.[69] For antibody and BSA modified device, we observed an increase of ~3.85 kΩ resistance for maximum stretching (6% tensile strain) and a decrease of ~ 2.84 kΩ resistance for maximum compression (6% compressive strain) of the device with respect to original state. Fig. S7a† and Fig. S7b† show the change in resistance ΔR (change in resistance of the device measured before and after exposure to HRP2 antigen) of the device for two different HRP2 concentrations, with different tensile and compressive strain, respectively. The change in resistance ΔR shows a very little initial inflexion for up to 0.05% strain followed by a trend towards saturation. These measurements were respectively carried out for each HRP2 concentration (at 6% strain) and similar trend of increase or decrease in resistance was observed for stretching or compression of the device, respectively. However, the change in resistance ΔR of the device was minimally effected on bending (Fig. 6a) and a maximum ~ 4 % change in ΔR was observed with respect to original unbend state of the device (Fig. 6b). This indicates endurance of the device with respect to mechanical strain.

Conclusions

In conclusion, we have demonstrated a flexible, light weight MWCNTs-ZnO nanofiber based chemiresistive biosensor for the label free detection of malaria biomarker HRP2.The CNTs-ZnO nanofibers were synthesized by a simple, low cost electrospinning technique and deposited between the pre patterned source and the drain electrodes on flexible substrate. The device utilizes unique properties of composite nanofiber channel, which provides a novel matrix for one step covalent conjugation of malaria HRP2 antibody without further surface modification. The fabricated chemiresistor exhibits good sensitivity of 8.29 kΩ g^{-1} mL in the wider detection range of 10 fg mL^{-1} -10 ng mL^{-1} of HRP2.These devices also

View Article Online
DOI: 10.1039/C7AN00243B

demonstrate good reproducibility and specificity to targeted malaria HRP2 antigen. This flexible chemiresistive platform has great potential in sensing of a host of several important biomarkers towards developing smart point-of-care diagnostic devices, touch sensors, and flexible electronics.

References

1 M. K. Sharma, V. K. Rao, G. S. Agarwal, G. P. Rai, N. Gopalan, S. Prakash, S. Sharma and R. Vijayaraghavan, *J. Clin. Microbiol.*, 2008, **46**, 3759–3765.

2 World Health Organization, *The world health report 2003: shaping the future*, World Health Organization, 2003.

3 C. K. Murray, R. A. Gasser, A. J. Magill and R. S. Miller, *Clin. Microbiol. Rev.*, 2008, **21**, 97–110.

4 C. M. Kifude, H. G. Rajasekariah, D. J. Sullivan, V. A. Stewart, E. Angov, S. K. Martin, C. L. Diggs and J. N. Waitumbi, *Clin. Vaccine Immunol.*, 2008, **15**, 1012–1018.

5 J. Hanson, S. W. Lam, K. C. Mahanta, R. Pattnaik, S. Alam, S. Mohanty, M. U. Hasan, A. Hossain, P. Charunwatthana and K. Chotivanich, *J. Infect. Dis.*, 2012, **206**, 571–579.

6 D. Warhurst and J. Williams, *J. Clin. Pathol.*, 1996, **49**, 533.

7 C. Erdman and J. W. Emerson, *Bioinformatics*, 2008, **24**, 2143–2148.

8 G. A. Fontecha, M. Mendoza, E. Banegas, M. Poorak, A. M. De Oliveira, T. Mancero, V. Udhayakumar, N. W. Lucchi and R. E. Mejia, 2012.

9 L. L. Poon, B. W. Wong, E. H. Ma, K. H. Chan, L. M. Chow, W. Abeyewickreme, N. Tangpukdee, K. Y. Yuen, Y. Guan and S. Looareesuwan, *Clin. Chem.*, 2006, **52**, 303–306.

10 S. Yatsushiro, S. Yamamura, Y. Yamaguchi, Y. Shinohara, E. Tamiya, T. Horii, Y. Baba and M. Kataoka, *PLoS One*, 2010, **5**, e13179.

11 L. Hein-Kristensen, L. Wiese, J. Kurtzhals and T. Staalsoe, *Exp. Parasitol.*, 2009, **123**, 152–157.

12 H. M. Shapiro and F. Mandy, *Cytometry A*, 2007, **71**, 643–645.

13 G. Campuzano-Zuluaga, T. Hänscheid and M. P. Grobusch, *Malar. J.*, 2010, **9**, 346.

14 P. A. Demirev, *Expert Rev. Mol. Diagn.*, 2004, **4**, 821–829.

15 E. Gikunoo, A. Abera and E. Woldesenbet, *Sensors*, 2014, **14**, 14686–14699.

16 M. de Souza Castilho, T. Laube, H. Yamanaka, S. Alegret and M. Pividori, *Anal. Chem.*, 2011, **83**, 5570–5577.

17 E. Banoth, V. K. Kasula and S. S. Gorthi, *Appl. Opt.*, 2016, **55**, 8637–8643.

18 B. Ding, M. Wang, X. Wang, J. Yu and G. Sun, *Mater. Today*, 2010, **13**, 16–27.

19 P.-C. Hsu, H. Wu, T. J. Carney, M. T. McDowell, Y. Yang, E. C. Garnett, M. Li, L. Hu and Y. Cui, *Acs Nano*, 2012, **6**, 5150–5156.

20 B. H. Lee, M. Y. Song, S.-Y. Jang, S. M. Jo, S.-Y. Kwak and D. Y. Kim, *J. Phys. Chem. C*, 2009, **113**, 21453–21457.

21 M. Ahmad, C. Pan, Z. Luo and J. Zhu, *J. Phys. Chem. C*, 2010, **114**, 9308–9313.

22 M. Ahmad, C. Pan and J. Zhu, *J. Mater. Chem.*, 2010, **20**, 7169–7174.

23 S.-Y. Lin, S.-J. Chang and T.-J. Hsueh, *Appl. Phys. Lett.*, 2014, **104**, 193704.

24 H. Hong, J. Shi, Y. Yang, Y. Zhang, J. W. Engle, R. J. Nickles, X. Wang and W. Cai, *Nano Lett.*, 2011, **11**, 3744–3750.

25 A. Vasudev, A. Kaushik and S. Bhansali, *Biosens. Bioelectron.*, 2013, **39**, 300–305.

26 M. A. Ali, K. Mondal, C. Singh, B. D. Malhotra and A. Sharma, *Nanoscale*, 2015, **7**, 7234–7245.

27 M. Das, G. Sumana, R. Nagarajan and B. Malhotra, *Thin Solid Films*, 2010, **519**, 1196–1201.

28 M. Tak, V. Gupta and M. Tomar, *Biosens. Bioelectron.*, 2014, **59**, 200–207.29Z. Zhao, X. Chen, B. Tay, J. Chen, Z. Han and K. A. Khor, *Biosens. Bioelectron.*, 2007, **23**, 135–139.

30 Z. Dai, G. Shao, J. Hong, J. Bao and J. Shen, *Biosens. Bioelectron.*, 2009, **24**, 1286–1291.

31 Y. Wei, Y. Li, X. Liu, Y. Xian, G. Shi and L. Jin, *Biosens. Bioelectron.*, 2010, **26**, 275–278.

32 K. B. Paul, S. Kumar, S. Tripathy, S. R. K. Vanjari, V. Singh and S. G. Singh, *Biosens. Bioelectron.*, 2016, **80**, 39–46.

33 M. Zhao, X. Wang, L. Ning, J. Jia, X. Li and L. Cao, *Sens. Actuators B Chem.*, 2011, **156**, 588–592.

34 C. Karuppiah, S. Palanisamy, S.-M. Chen, V. Veeramani and P. Periakaruppan, *Sens. Actuators B Chem.*, 2014, **196**, 450–456.

35 R. Singh, A. Sharma, S. Hong and J. Jang, *Analyst*, 2014, **139**, 5415–5421.

36 J. J. Gooding, *Electrochimica Acta*, 2005, **50**, 3049–3060.

37 A. Liu, *Biosens. Bioelectron.*, 2008, **24**, 167–177.

38 J. Khanderi, R. C. Hoffmann, A. Gurlo and J. J. Schneider, *J. Mater. Chem.*, 2009, **19**, 5039–5046.

39 M. Samadi, H. A. Shivaee, M. Zanetti, A. Pourjavadi and A. Moshfegh, *J. Mol. Catal. Chem.*, 2012, **359**, 42–48.

40 B. Haghighi and S. Bozorgzadeh, *Talanta*, 2011, **85**, 2189–2193.

41 Y. Wang, L. Yu, J. Wang, L. Lou, W. Du, Z. Zhu, H. Peng and J. Zhu, *J. Electroanal. Chem.*, 2011, **661**, 8–12.

42 S. Palanisamy, S. Cheemalapati and S.-M. Chen, *Anal. Biochem.*, 2012, **429**, 108–115.

43 B. Fang, C. Zhang, W. Zhang and G. Wang, *Electrochimica Acta*, 2009, **55**, 178–182.

44 Z. Zhang, C. Shao, X. Li, C. Wang, M. Zhang and Y. Liu, *ACS Appl. Mater. Interfaces*, 2010, **2**, 2915–2923.

45 M. Tak, V. Gupta and M. Tomar, *J. Mater. Chem. B*, 2013, **1**, 6392–6401.

46 Rajesh, V. Sharma, N. K. Puri, R. K. Singh, A. M. Biradar and A. Mulchanadani, *Appl. Phys. Lett.*, 2013, **103**, 203703.

47 M. Durga Prakash, S. R. K. Vanjari, C. S. Sharma and S. G. Singh, *Sensors*, 2016, **16**, 1354.

48 D. P. Matta, S. Tripathy, S. R. K. Vanjari, C. S. Sharma and S. G. Singh, *Biomed. Microdevices*, 2016, **18**, 111.

49 H. Shafiee, W. Asghar, F. Inci, M. Yuksekkaya, M. Jahangir, M. H. Zhang, N. G. Durmus, U. A. Gurkan, D. R. Kuritzkes and U. Demirci, *Sci. Rep.*, 2015, **5**, 8719.

50 C. Desmet, C. A. Marquette, L. J. Blum and B. Doumèche, *Biosens. Bioelectron.*, 2016, **76**, 145–163.

51 S. Kumar, A. Sen, S. Kumar, S. Augustine, B. K. Yadav, S. Mishra and B. D. Malhotra, *Appl. Phys. Lett.*, 2016, **108**, 203702.

52 Y. Zhu, X. Xu, N. D. Brault, A. J. Keefe, X. Han, Y. Deng, J. Xu, Q. Yu and S. Jiang, *Anal. Chem.*, 2014, **86**, 2871–2875.

53 M. Costa, B. Veigas, J. Jacob, D. Santos, J. Gomes, P. Baptista, R. Martins, J. Inácio and E. Fortunato, *Nanotechnology*, 2014, **25**, 094006.

54 W. Li, L. Li, S. Ge, X. Song, L. Ge, M. Yan and J. Yu, *Biosens. Bioelectron.*, 2014, **56**, 167–173.

55 Y. Liu, H. Zhang, X. An, C. Gao, Z. Zhang, J. Zhou, M. Zhou and E. Xie, *J. Alloys Compd.*, 2010, **506**, 772–776.

View Article Online
DOI: 10.1039/C7AN00243B

56 Q. Li, Y. Li, X. Zhang, S. B. Chikkannanavar, Y. Zhao, A. M. Dangelewicz, L. Zheng, S. K. Doorn, Q. Jia and D. E. Peterson, *Adv. Mater.*, 2007, **19**, 3358–3363.
57 K. Behler, S. Osswald, H. Ye, S. Dimovski and Y. Gogotsi, *J. Nanoparticle Res.*, 2006, **8**, 615–625.
58 M. Hossain, H. Shima, M. A. Islam, M. Hasan and M. Lee, *RSC Adv.*, 2016, **6**, 4683–4694.
59 K. Hemalatha, A. Prakash, K. Guruprakash and M. Jayakumar, *J. Mater. Chem. A*, 2014, **2**, 1757–1766.
60 G. Hu, X. Meng, X. Feng, Y. Ding, S. Zhang and M. Yang, *J. Mater. Sci.*, 2007, **42**, 7162–7170.
61 M. Nazir, I. I. Naqvi, Americ. J. Anal. Chem. 2013, 4, 134 –140.
62 W. H. Nam, B. B. Kim, S. G. Seo, Y. S. Lim, J.-Y. Kim, W.-S. Seo, W. K. Choi, H.-H. Park and J. Y. Lee, *Nano Lett.*, 2014, **14**, 5104–5109.
63 W. H. Nam, B. B. Kim, Y. S. Lim, W. Seo, H. Park and J. Y. Lee, *J. Am. Ceram. Soc.*, 2016, **99**, 2077–2082.
64 J. W. Park, D. H. Kim, S.-H. Choi, M. Lee and D. Lim, *J. Korean Phys. Soc.*, 2010, **57**, 1482–1485.
65 Y. Cui, Q. Wei, H. Park and C. M. Lieber, *Science*, 2001, **293**, 1289–1292.
66 A. Stafiniak, B. Boratyński, A. Baranowska-Korczyc, A. Szyszka, M. Ramiączek-Krasowska, J. Prażmowska, K. Fronc, D. Elbaum, R. Paszkiewicz and M. Tłaczała, *Sens. Actuators B Chem.*, 2011, **160**, 1413–1418.
67 A. B. Artyukhin, M. Stadermann, R. W. Friddle, P. Stroeve, O. Bakajin and A. Noy, *Nano Lett.*, 2006, **6**, 2080–2085.
68 N. Puri, A. Niazi, A. M. Biradar, A. Mulchandani and Rajesh, *Appl. Phys. Lett.*, 2014, **105**, 153701.
69 X. Liao, Z. Zhang, Q. Liao, Q. Liang, Y. Ou, M. Xu, M. Li, G. Zhang and Y. Zhang, *Nanoscale*, 2016, **8**, 13025–13032.

View Article Online
DOI: 10.1039/C7AN00243B

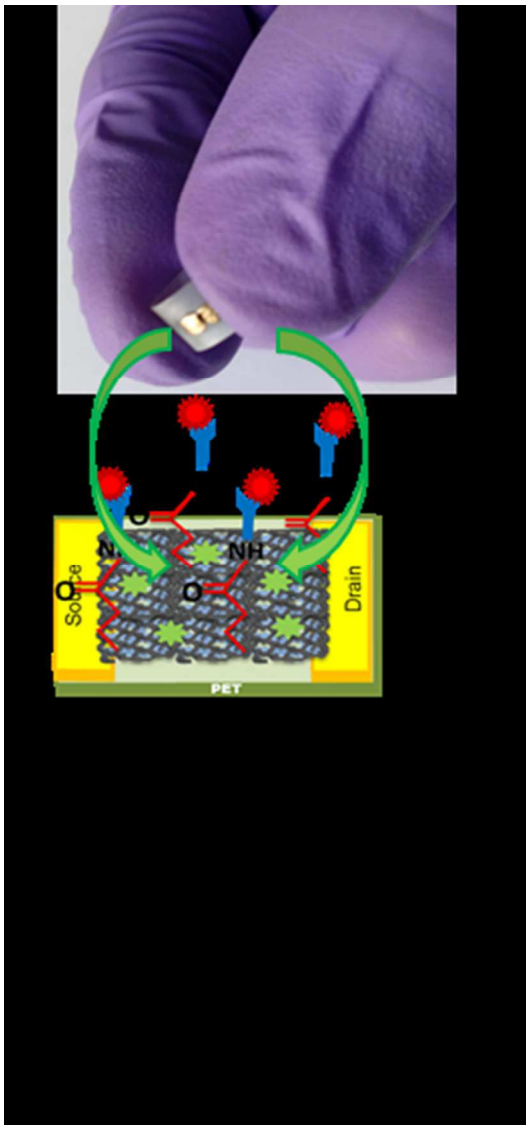

44x94mm (150 x 150 DPI)